J Mater Sci: Mater Med (2008) 19:2735–2741
DOI 10.1007/s10856-008-3396-3

# Novel fabrication of nano-rod array structures on titanium and in vitro cell responses

**Yongxing Liu · Weihui Chen · Yunzhi Yang · Joo L. Ong · Kanji Tsuru · Satoshi Hayakawa · Akiyoshi Osaka**

Received: 31 March 2006 / Accepted: 31 January 2008 / Published online: 29 February 2008


**Abstract** Nano-scale rod arrays of titania were fabricated on titanium surface by a glass phase topotaxy growth (GPT) method, which was featured by an interfacial reaction between sodium tetraborate coating and the preheated metallic titanium at elevated temperature. The samples were characterized by thin-film X-ray diffraction (XRD), scanning electron microscope (SEM), profilometer and contact angle measurement. Thin-film XRD analysis indicated that the nano-rod arrays were composed of pure rutile titania phase. SEM images showed that these rutile rods were 100–200 nm wide and 1–2 μm long. The nano-rod arrays had significantly higher average roughness ($P < 0.05$) and greater hydrophilicity ($P < 0.05$) compared to the control. Human embryonic palatal mesenchymal (HEPM) cells were grown to evaluate in vitro cell responses to the nano-rod array structures in terms of cell attachment and proliferation. An equivalent high attachment rate of 94% was observed after 4-h incubation, but a lower proliferation rate was observed on the nano-rod array after 12-day culture compared to the control ($P < 0.05$).

Y. Liu (✉) · W. Chen · Y. Yang · J. L. Ong
Department of Biomedical Engineering and Imaging,
The University of Tennessee Health Science Center,
920 Madison Ave suite 1005, Memphis, TN 38163, USA
e-mail: yliu28@utmem.edu

W. Chen
Department of Oral Maxillofacial Surgery, Fujian Medical University, Fuzhou 350001, China

K. Tsuru · S. Hayakawa · A. Osaka
Faculty of Engineering, Okayama University,
Okayama-shi 700-8530, Japan

## 1 Introduction

Commercially pure titanium (c.p. Ti) and its alloys have been widely used in dental and orthopedic implants for their high fracture toughness and excellent biocompatibility. However, the lack of bioactivity results in non-direct bonding between bone and Ti implants, which accounts for the loosening and failure of some implants in the long term. Thus quite a range of research has been conducted aiming to impart bioactivity to titanium implants or enhance directly mechanical fixation [1–11]. In addition to surface chemistry, surface structures of implants have been reported to play a unique role in the bone-biomaterials interactions [1–8]. In particular, nano-scale topography demonstrated significant effects on cell responses which implied a new approach to regulate cell behaviors by simply manipulating implant surface structures [6]. The available techniques for fabricating such micro and nano-scale features typically involve lithography methodology which was also known for a few limitations including high cost, requirement for high-level smoothness of the sample, and difficulty in applying to the complex-shaped objects such as titanium implants [6]. A recent methodology involves the crystallization and de-mixing of copolymers [7, 8] which is convenient but applicable only to the specific polymers. Its applications to titanium implants were not yet displayed.

Glass phase topotaxy (GPT) approach was recently reported as a new technique to fabricate arrays of submicron and nano scale titania rods by applying sodium borate glass to titanium substrates at elevated temperature [12–15]. One of the key steps in that technique was making glass which involved a high temperature process (1100°C). It makes the technique less convenient. In addition, the coverage of the as-evolved array structures was low and

constrained only to some random regions; Large-scale homogeneity was not achieved [12]. These limitations definitely restrict this technique from practical applications. In order to overcome these problems, major developments were made in this study where a commercially-available sodium tretraborate powders was elected for the coating material in replace of the borate glasses as those used in previous reports [12–15]; and titanium substrates were subject to a series of heat treatment before the glass phase topotaxy growth in order to control the interfacial reaction between coatings and titanium surface. The optimal processing parameters and homogenous nano-rod array structures were correlated. Cell responses to the homogenous nano-rod array structures were evaluated.

## 2 Materials and methods

### 2.1 Materials

Commercially pure titanium disks (Tico Titanium Inc., Oak Ridge North, TX, USA) with 12 mm in diameter and 0.5 mm in thickness were ground using 400 grit grinding paper and preheated at 700°C in air in an electric furnace (Thermolyne 48000, Barnstead international, Dubuque, IO, USA) for 1, 2, 3 and 4 h. Reagent grade sodium tetraborate powder (denoted as NB hereafter) were purchased from Fisher Scientific Inc. (Pittsburgh, PA, USA), dehydrated and dried at 300°C for 10 h in an electric furnace (Thermolyne 48000, Barnstead international, Dubuque, IO, USA) before use. The as-dried NB powder was mixed with anhydrous ethanol to make slurry which was dropped onto the preheated titanium disks. After drying off the ethanol in air, a loose NB coating of about 1 mm thick was made on the disks. These samples were placed in the furnace and heated up to 700°C at the rate of 10°C/min; dwelled for 5 h. After cooling down to room temperature at a rate of 5°C/min, the NB-coated samples were immersed in 80°C water for 5 h, followed by ultrasonic cleaning and thoroughly rinsing in distilled water to remove the loose coating material. Samples were then dried in air and kept in partial vacuum environment until use.

Preheating treatment was conducted at 700°C because it was proved the effective oxidization temperature for titanium in our preliminary experiments. On another hand, higher temperature than 700°C is not applicable because it may readily over oxidize the titanium disk.

### 2.2 Characterization

Microstructures of the substrate were observed by a scanning electron microscope (SEM, Philips XL 30, Philips Electron Optics, The Netherlands) operated at 15 kV acceleration voltage and 40 mA emission current after coating 30 nm thick gold. Elemental analysis was conducted by the energy dispersive X-ray spectroscopy (EDX) attached with the microscope. Crystalline phases were identified using a D8 Advance X-ray diffractometer (Bruker AXS Inc., Madison WI, USA ) scanning in thin-film mode and at a rate of 0.01°/s. Average roughness (Ra) of sample surface was measured at length of 4 mm and cut-off value 0.80 mm using a profilometor (Surtronic 25, Taylor Hobson Inc., West Chicago, IL, USA). Contact angle toward water was measured using a video contact angle goniometer (VCA-Optima, AST products Inc., Billerica, MA, USA). Statistical analysis was conducted by using One-way ANOVA at a significance level of $P < 0.05$.

### 2.3 Cell attachment and proliferation

The samples with homogenous nano-rod structures were elected to evaluate cell responses, i.e., samples derived from disks preheated for 3 h and followed by NB treatment. Correspondingly, the substrates preheated for 3 h without further NB treatment were used as controls.

ATCC CRL 1486 human embryonic palatal mesenchymal cells (HEPM; ATCC, Manassas, VA, USA), an osteoblast precursor cell line, were used to evaluate initial cell attachment and cell proliferation. The culture medium was composed of Dulbecco's modified Eagle's medium (DMEM), supplemented with 3% fetal bovine serum (FBS), 1% L-Glutamin (200 mM), 1% antibiotic-antimycotic solution (PSA: 10,000 units/ml penicillin G sodium, 10,000 μg/ml streptomycin sulfate, 25 μg/ml amphotericin B), 10 μM dexamethasone, 50 μg/ml L-Ascrobic acid and 10 mM $\beta$-glycerophosphate.

Cells were seeded on samples at a density of $2 \times 10^4$ cells/sample and incubated in a 5% $CO_2$ humidified incubator at 37°C. The number of attached cells was examined after 0.5, 1, 2, 3 and 4 h incubation. Briefly, at each time point, rinse the surfaces with phosphate buffered saline (PBS) to remove non-attached cells. Rinsing was performed two times and the medium was collected for measuring the non-attached cells. The number of non-attached cells was counted using a coulter counter (Z2 Coulter, Beckman Coulter Inc., Fullerton, CA, USA), and the number of attached cells was computed by subtracting the non-attached cell number from the initial seeding number.

Cell proliferation over a period of 12 days was examined by measuring double stranded deoxyribonucleic acid (dsDNA) content which is proportional to the cell numbers. Culture media was replaced every four days. Samples were collected on day 2, 4, 8 and 12. Briefly, after removing the

supernatants and washing with 1 ml PBS, samples were lysed by freeze-thaw method for 3 times, followed by ultrasonication in 1 ml 0.2% Triton X-100 (Fisher Scientific Inc, Houston, TX) for 5 min. The triton lysates were stored at −20°C until assay. dsDNA content was measured by a fluorometric quantification method using PicoGreen assay (Molecular Probe, Gene, OR). According to the manufacturer's instruction, 50 µl aliquot of the triton lysate was added to 50 µl working reagent. Sample fluorescence emissions at 485 nm were read with the excitation set at 528 nm on an FL × 800 microplate fluorescence reader (Bio-tek Instruments Inc., Winooski, VT). dsDNA content were determined by comparing fluorescent reading to the dsDNA standard curves. One-way ANOVA was used to analyze the differences in cell proliferation with a significance level of $P < 0.05$.

### 2.4 Cell morphology

Cell morphology was examined by SEM microscopy. After 2 h and 24 h incubation, the culture media were removed and samples were rinsed three times with PBS, fixing with 4% paraformaldehyde for 30 min. After fixation, the samples were rinsed with PBS for 15 min and sequentially dehydrated for 15 min in each 50, 75, 90, and 100% ethanol. Before viewing on SEM, samples were dried on a $CO_2$ critical point dryer (Tousimis Samdri 790, Tousimis Research Corp., Rockville, MD) and coated with 30 nm gold. To quantitate changes in cell size with time, cell diameters were measured on SEM micrographs of cells cultured for 2 h. Cell diameters were measured and averaged on 90 cells. One-way ANOVA was used to analyze the differences in cell size with a significance level of $P < 0.05$.

## 3 Results

### 3.1 Chemistry and crystalline phases

Thin film X-ray diffraction for titanium disks preheated at 700°C displayed the dominance of a rutile titania phase on the surface. Diffraction patterns in Fig. 1a showed intense peaks at 27.5° and 36.1° (2 theta) which were assigned to the diffraction from (110) and (101) planes of rutile titania (PDF #21-1276). The peaks at 38° and 40° (2 theta) were attributable to metallic α-titanium (PDF#44-1294) background due to the penetration of X-ray into the deeper layer of titanium disks. Apparently, the diffraction from α-titanium phase decreased in intensity as the heating time increased, indicating the increase in thickness of the rutile layer as the heating time extended.

After these preheated disks were further treated with NB coating at 700°C for various time, rutile titania became the only detectable crystalline phase on the surface and no α-titanium phases were detected (Fig. 1b). X-ray diffraction patterns showed sharp and strong diffraction peaks at 27.48° attributed to (110) plane of rutile titania. Moreover, EDX analysis detected only titanium and oxygen elements on the surface with a molar ratio of 1:2. This indicated that the surface was clear of other compounds other than rutile titania.

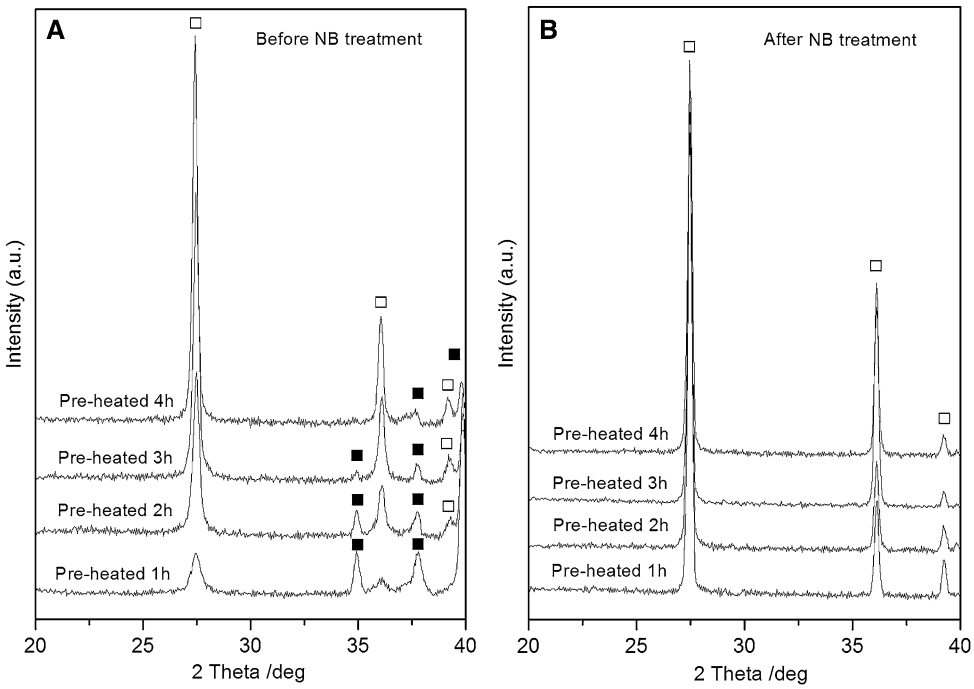


**Fig. 1** XRD patterns for titanium disks (**a**) preheated at 700°C for 1, 2, 3 and 4 h, and (**b**) further treated by NB coating after preheated at 700°C for 1, 2, 3 and 4 h

### 3.2 Surface morphology

Titanium disks showed similar morphology after preheated at 700°C in air for up to 4 h, as displayed representatively in Fig. 2a. Heat treatment produced a dense rutile layer on titanium surface composed of compact, submicron-sized rutile crystals (according to XRD analysis in 3.1) independent on heating time. Nevertheless, different microstructures were evolved directly related to the preheating time after further treatment with NB coating. On substrates preheated for 1 and 2 h, a mixture of submicron- and micron-scale, irregular-shaped rutile crystals were produced on the surface (representatively shown in Fig. 2b). In contrast, on the titanium disks preheated for 3 and 4 h, homogenous, nano-scale rutile rods of 100–200 nm wide and 1–2 microns long were obtained. The typical morphology was displayed in Fig. 2c. All the nano-scale rods displayed clear elongated cubic habit, covering homogenously on the surface and projecting approximately upright. It is noteworthy that rutile rod arrays on all of the NB-treated samples covered completely the disk surface.

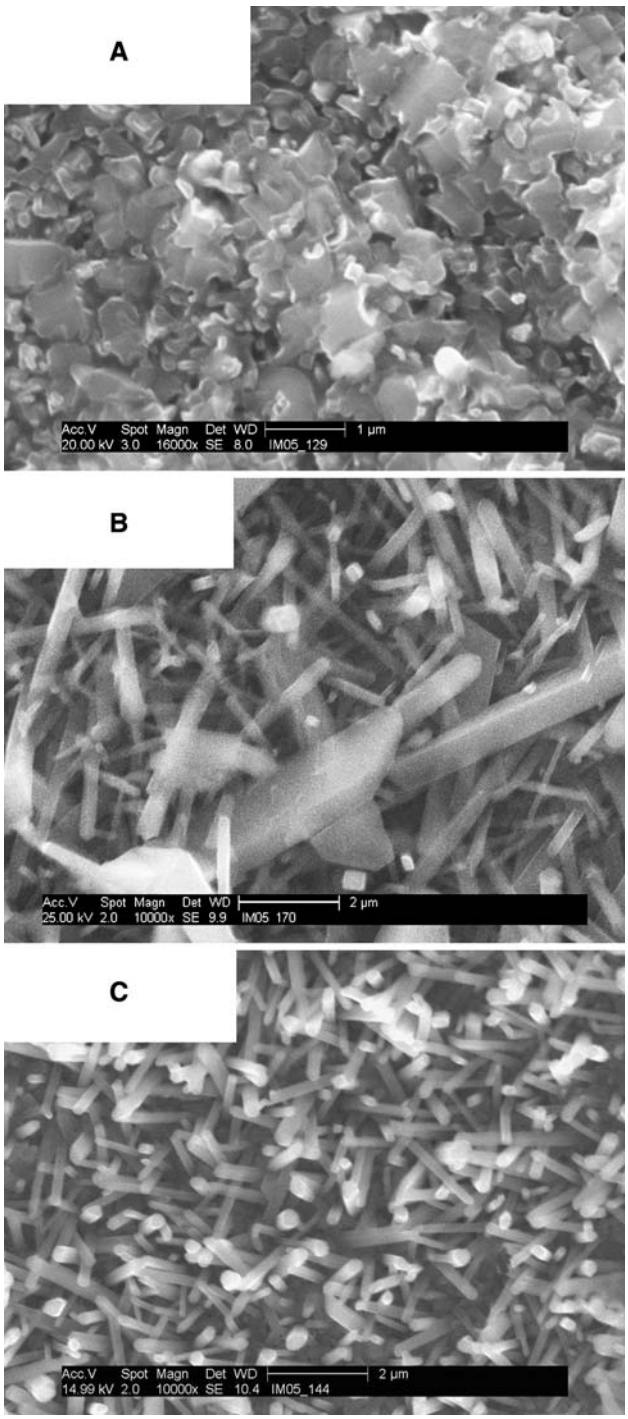


**Fig. 2** Scanning electron microscopy images for the samples (**a**) titanium disks preheated at 700°C for 3 h, (**b**) NB treated titanium disks after preheated at 700°C for 1 and 2 h, and (**c**) NB treated titanium disks after preheated at 700°C for 3 and 4 h

### 3.3 Surface roughness and contact angle

Samples having homogenous nano-rod array structures were measured for surface average roughness (Ra) and the result was shown in Fig. 3a. It read 0.33 ± 0.04 µm for nano-rod arrays which was significantly higher ($P < 0.05$) than that of control (0.20 ± 0.01 µm). Moreover, nano-rod

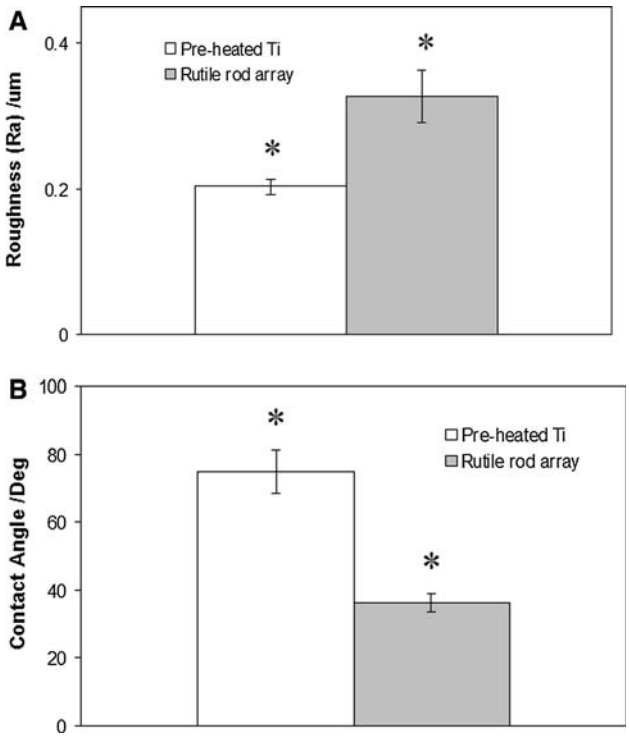


**Fig. 3** Average surface roughness (**a**) and contact angle toward water (**b**) of the control and nano-rod array. *Indicates significantly different ($P < 0.05$)

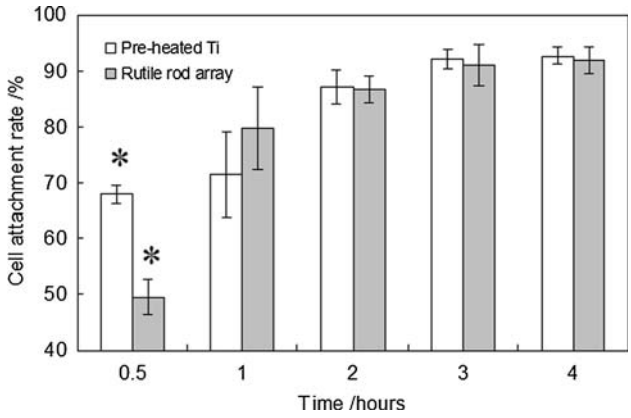


**Fig. 4** Graphs for the cell attachment rates on the control and nano-rod array. *Indicates significantly different ($P < 0.05$)

arrays demonstrated a remarkably higher hydrophilicity ($P < 0.05$) measuring $36.3 \pm 2.8°$ of the contact angle compared to $75.0 \pm 6.4°$ for the control as displayed in Fig. 3b.

### 3.4 Cell attachment

Cell attachment rates were measured illustrated in Fig. 4. No significant difference ($P > 0.05$) in attachment rate was observed on nano-rod arrays and control after incubation for 1 h, although a relatively higher ($P < 0.05$) rate was observed on the control in the initial 30 min. At 4-h incubation cell attachment rates reached 92% on both nano-rod arrays and control, and no significant difference was observed ($P > 0.05$).

### 3.5 Cell morphology

Cells displayed similar morphology on both surfaces after 2 and 24 h incubation. At 2 h of incubation, cells on both surfaces displayed early stage growth from round/spherical morphology to flattened morphology. Some cells apparently sent out processes that might begin to form lamellipodia (Fig. 5a, b). The remarkable difference in morphology was quantified cell sizes. Cells on the nano-rod arrays had significantly smaller diameter averaging $23 \pm 9$ μm compared to $27 \pm 11$ μm of those grown on the control ($P < 0.05$). The percentage of cells with diameter larger than 40 μm was also less on the nano rod array, comparing 3% on the array to 13% on the control ($P < 0.01$). After 24 h incubation, all cells appeared flattened and spread across on both surfaces. Cell margins merged into neighboring cells making it hard to discriminate single cell (Fig. 5c, d).

### 3.6 Cell proliferation

dsDNA content synthesized by HEMP cells increased continuously from about 300 ng/ml on day 2 up to >1000 ng/ml on day 12 in both the nano-rod array and

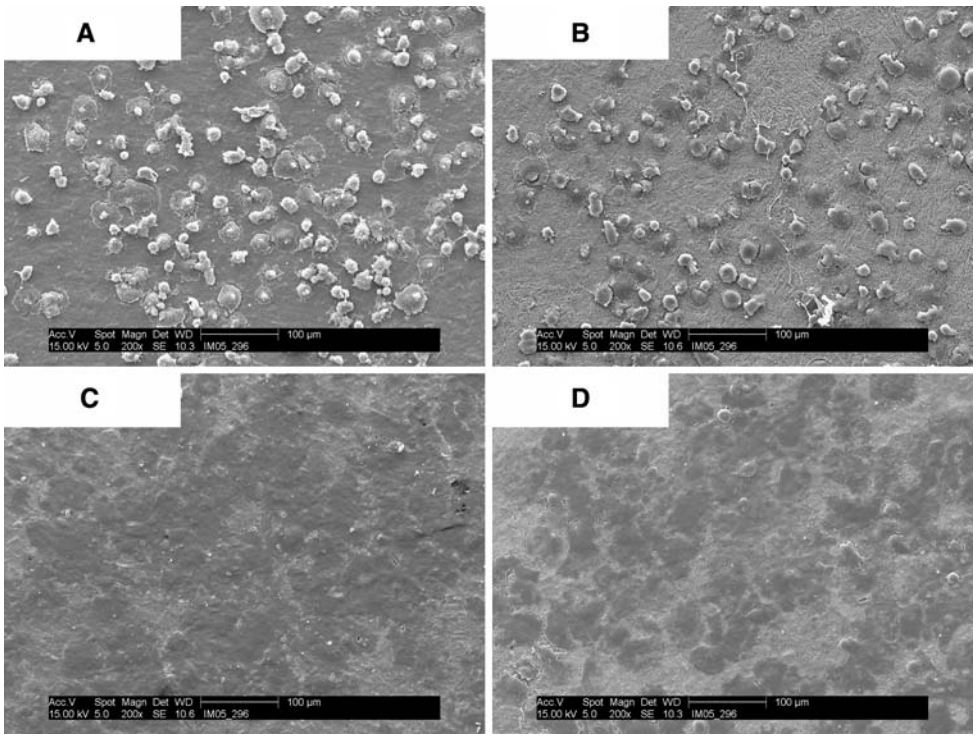


**Fig. 5** Scanning electron microscopy images for cells incubated on the control ad nano-rod array for: (**a**) 2 h on control, (**b**) 2 h on nano-rod array, (**c**) 24 h on control, and (**d**) 24 on nano-rod array

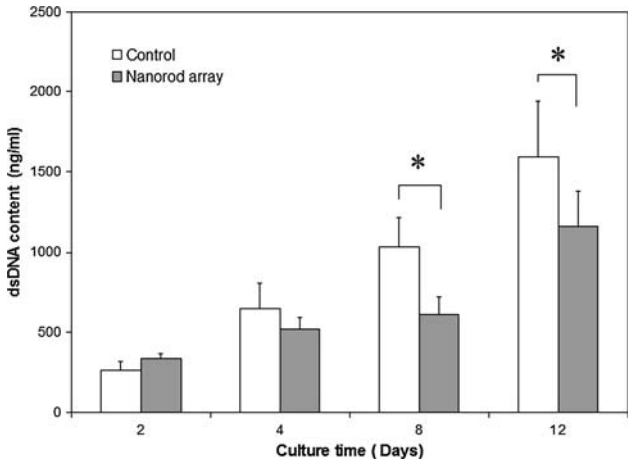


**Fig. 6** Graphs for the dsDNA content synthesized by cells cultured on the control and nano-rod array for up to 12 days. *Indicates significantly different ($P < 0.05$)

control group. dsDNA content was not significantly different in two groups before day 4 ($P > 0.05$), however, after then, the dsDNA content became significantly lower on nano-rod array group compared to the control ($P < 0.05$ on day 8 and 12) (See in Fig. 6).

## 4 Discussion

### 4.1 Nano-rod array structures

Surface structures of implants are known of playing significant roles in the interactions between living bone tissues and implants [1–8]. Particularly, nano-scale features have attracted ever increasingly attention due to their unique effects on in vitro cell responses and proposed in vivo responses [6]. Thus various microfabrication technologies have been investigated to examine the effects of micro features. However, most of these techniques are not applicable to titanium implants. Recently, a new technique, namely glass phase topotaxy growth (GPT), was reported which displayed the feasibility to modify directly the surface of titanium implants for nano-scale features [12–15]. Nevertheless, the as-reported GPT technique encountered limitations such as lack of homogeneity and requirement for very-high temperature (1100°C for making glasses) [12]. As a major development, the present experiment employed a commercially available sodium tetraborate (NB) powder to avoid the glass-making process. The NB powder is crystalline phase of sodium tetraborate which is distinctively crystallographically different from sodium tetraborate glass used in previous experiments. Nevertheless, it turned out that the crystalline NB interacted also effectively with preheated titanium and successfully produced homogenous nano rod arrays of rutile on the titanium disks. It implied that it is the chemistry of sodium tetraborate accounts for the GPT growth of rod arrays not the crystallographic property.

According to GPT hypothesis, metallic titanium might dissolve into the sodium borate coating at such a high rate that the melting point (T*l*) and glass transition temperature (T*g*) of the coating was a quickly decreased. As a result, a glassy layer was formed on the titanium surface which could have suppressed oxygen diffusion and depressed the GPT growth [16–19]. Based on also our preliminary experiments, we proposed that a moderate dissolution rate for titanium might overcome the suppression effect and in turn favor the GPT growth of smaller-sized and more homogenous rutile rods. As a solution, titanium disks were preheated to produce a more chemically-stable rutile layer on which the NB was then coated. This design proved remarkably effective in producing homogenous nano-rod arrays given the preheating treatment was sufficient, i.e., preheating titanium disks at 700°C for no less than 3 h in air. In contrast, preheating for less than 3 h produced thinner rutile layer (proved by weaker XRD diffraction shown in Fig. 1a), which eventually failed to moderate effectively the dissolution rate and resulted in non-homogenous rods.

The nano-rod array displayed higher surface roughness and hydrophility ($P < 0.05$). This was apparently attributed to the nano structures given its chemistry is same to the control. A larger surface area is apparent compared to the control though the quantitative analysis was not presented in this study. Higher hydrophility is attributable to the higher surface roughness as described by Wenzel [20], i.e., when the contact angle is lower than 90° for a material, it will inevitably be decreased when the surface roughness is increased. Thus, a more hydrophilic surface due to nano-rod structures was observed on the nano-rod arrays.

### 4.2 Cell responses

It is known that cells response directly to topographies, regarding attachment, migration, differentiation, extracellular matrix production and many others [6]. Rough surface was reported to induce bone formation on titanium implants in vivo in contrast smooth surface did not [21]. Better cell attachment on rough surfaces was reported by in vitro studies in comparison to smooth surface [22–24]. In particular, nano-featured surfaces of metal and ceramics were reported to promote osteoblast or osteoblast-like cell attachment [23, 24]. In the present study, it was displayed however the initial cell attachment rate on the nano-rod array was not significantly different in 1-h incubation compared to the control ($P > 0.05$). A comparable high attachment rate of 92% was obtained on both the nano-rod array and control after incubating 4 h ($P > 0.05$).

SEM observation displayed that cells had similar flattened morphology on the nano-rod array and control after 24-h incubation. This observation was inconsistent with the report by Kim et al. [9] in which MG-63 cells projected more cytoplasmic processes and changed more into cuboidal shapes on the rougher surface indicating more differentiation to osteoblast. This inconsistency in two observations may be attributable to the great difference in roughness level of the tested samples (0.20–0.33 μm in the present experiment versus 2.95 μm in their experiment). This implied that nano-rod arrays affected more like a smooth surface other than a rough surface on the morphometric responses of HEPM cells. This may also explain the comparable high attachment rates on rod arrays compared to control.

It was noticed, however, that cells on rod arrays had smaller average size after 2-h incubation compared to the control. The smaller cell size indicated a possible slower growth rate on the nano-rod arrays compared to the smoother control surface [9]. This postulation was supported by the longer-term proliferation. After culturing up to 12 days, cells grew significantly less on the nano-rod array measuring the dsDNA content ($P < 0.05$ on day 8 and 12) compared to control. This observation complied well with other studies in which surface roughness impacted negatively on cell proliferation [25]. It is noteworthy, however, a lower proliferation rate does not necessarily imply less differentiation or secretory functions. In fact, an increase in differentiation and extracellular matrix production was observed in correlation to a decrease in proliferation and ALP activity on rough surfaces [25]. Thus it is possible that the nano-rod array stimulated HEPM differentiation and extracellular matrix production whereas suppressed the proliferation. The remarkable impact of surface structures on cell behaviors was tentatively attributed to the direct morphological effects or absorption of bioactive molecules from media and serum though the mechanism is yet clear so far [9, 23–26]. Future experiments will be conducted to evaluate the long-term effects of the nano-rod arrays on HEPM cell differentiation and secretary functions.

## 5 Conclusions

This study reported a developed glass phase topotaxy growth of nano-rod array structures on titanium surface. By controlling the preheating treatment and applying new coating materials, homogenous large-coverage nano-rod arrays were fabricated on titanium surface which were composed of pure rutile titania phase. The nano-rod array structures significantly increased the average roughness and hydrophility ($P < 0.01$) of titanium surface compared to the control. In vitro culture of HEPM cells displayed a comparable high initial attachment rate on the nano-rod arrays than control in 4-h incubation. However, the cell proliferation rate was significantly lower on the nano-rod arrays than control in 12-day culture. Future study is needed to evaluate the long-term in vitro responses of HEPM cells including differentiation and secretory functions.

## References


1. P.F. Chauvy, C. Mador, D. Landolt, Surf. Coat. Technol. **110**, 48 (1998)
2. C. Hallgren, H. Reimers, D. Chakarov, J. Gold, A. Wennerberg, Biomaterials **24**, 701 (2003)
3. J. Lincks, B.D. Boyan, C.R. Blanchard, C.H. Lohmann, Y. Liu, D.L. Cochran, D.D. Dean, Z. Schwartz, Biomaterials **19**, 2219 (1998)
4. Z. Schwartz, B.D. Boyan, J. Cell Biochem. **56**, 340 (1994)
5. K. Anslme, M. Bigerelle, B. Noel, A. Iost, P. Hardouin, J. Biomed. Mater. Res. **60**, 529 (2002)
6. R.G. Flemming, C.J. Murphy, G.A. Abrams, S.L. Goodman, P.F. Nealy, Biomaterials **20**, 573 (1999)
7. M.J. Dalby, D. Giannaras, M.O. Riehle, N. Gaegaard, S. Affrossman, A.S.G. Curtis, Biomaterials **25**, 77 (2004)
8. N.R. Washburna, K.M. Yamadab, C.G. Simon, S.B. Kennedya, E.J. Amisa, Biomaterials **25**, 1215 (2004)
9. H.J. Kim, S.H. Him, M.S. Him, E.J. Lee, H.G. Og, W.M. Oh, S.W. Park, W.J. Kim, G.J. Lee, N.G. Choi, J.T. Koh, D.B. Dinh, R.R. Hardin, K. Johnson, V.L. Sylvia, J.P. Schmitz, D.D. Dean, J. Biomed. Mater. Res. **74A**, 366 (2005)
10. C. Ohtsuki, H. Iida, S. Hayakawa, A. Osaka, J. Biomed. Mater. Res. **35**, 39 (1997)
11. Q. Liu, J. Ding, F.K.M. Stephanie, L. Wunder, G.R. Baran, Biomaterials **23**, 3103 (2002)
12. Y. Liu, K. Tsuru, S. Hayakawa, A. Osaka, J. Ceram. Soc. Jpn. **112**, 567 (2004)
13. S. Hayakawa,Y. Liu, K. Tsuru, K. Okamoto, A. Osaka, *Nanoscale Materials Science in Biology and Medicine*. Materials Research Society Symposia Proceedings, vol. 845 (Warrendale, PA, 2005) p. AA6.9
14. Y. Liu, K. Tsuru, S. Hayakawa, A. Osaka, J. Ceram. Soc. Jpn. **112**, 453 (2004)
15. Y. Liu, K. Tsuru, S. Hayakawa, A. Osaka, J. Ceram. Soc. Jpn. **112**, 634 (2004)
16. I.N. Anikin, I.I. Naumova, G.V. Ruyantseva, Sov. Phys. Crystallogr. **10**, 172 (1965)
17. A.J. Easteal, D.J. Udy, J. Inorg. Nucl. Chem. **35**, 3041 (1973)
18. F. Kawanura, I. Yasui, I. Sunagawa, J. Cryst. Growth **233**, 517 (2001)
19. J.S. Berkes, W.B. White, R. Roy, J. Appl. Phys. **36**, 3276 (1965)
20. R.N. Wenzel, Int. Eng. Chem. **28**, 988 (1936)
21. K. Tomas, S. Cook, J. Biomed. Mater. Res. **19**, 875 (1981)
22. K. Bowers, J. Keller, B. Randolph, D. Wick, C. Michaels, Int. J. Oral Maxillofac. Implants. **7**, 302 (1992)
23. T.J. Webster, J.U. Ejiofor, Biomaterials **25**, 4731 (2004)
24. T.J. Webster, E.L. Hellenmeyer, R.L. Price, Biomaterials **26**, 953 (2005)
25. J.Y. Matin, Z. Schwartz, T.W. Hummert, D.M. Schrub, J. Simpson, J. Lankford, D.D. Dean, D.L. Cochran, B.D. Boyan, J. Biomed. Mater. Res. **29**, 389 (1995)
26. S. Lossdofer, Z. Schwartz, L. Wang, C.H. Lohmann, J.D. Turner, M. Wieland, D.L. Cochran, B.D. Boyan, J. Biomed. Mater. Res. **70A**, 361 (2004)